Empirical model for the temporally resolved temperatures of post-detonation fireballs for aluminized high explosives

J. Motos Gordon*, Kevin C. Gross†, Glen P. Perram‡
Department of Engineering Physics, Air Force Institute of Technology
2950 Hobson Way, WPAFB, OH USA 45433-7765

ABSTRACT

A physics-based empirical model is developed to characterize the time varying temperature profile from post-detonation combustion. Fourier-transform infrared signatures are collected from field detonations of RDX-based aluminized high explosives surrounded by an aluminized plastic-bonded spin-cast liner. The rate of change of temperature in the post-detonation combustion fireballs are modeled using a radiative cooling term and a double exponential combustion source term. Optimized nonlinear least-squares fit of the numerical solution of the empirical model to the temperature data yields peak temperatures of 1290-1850. The observed heat released in the secondary combustion is well correlated with the high explosive and liner heat of combustion with an average efficiency of 54%.

Keywords: fireball temperature, radiative cooling, detonation, RDX, spectra

1. INTRODUCTION

The explosion of conventional munitions represents an intense visible and infrared emission event. The emitted radiation signatures can reveal a wealth of information regarding the explosion. Visible signatures can provide clues about the extent of the fireball and even the energy of the explosion [1]. Richer still, infrared spectral signatures can harbor information such as the type or class of explosive, the constituents of the explosive, the temperature of the detonation, and also the energy released. Robust classification of detonation events is predicated on the fundamental understanding of the physical phenomenology involved. However, methods are needed that do not require large amounts of time or extensive computational resources such as those found in chemical and hydrodynamic analysis. Recently, feature discrimination techniques and physics-based models have been able to differentiate between disparate explosive types and configurations and even static versus airdropped munitions. [2] Despite recent advances, the ability to differentiate between spectral features from very similar classes of explosives (i.e., RDX-based) has proven difficult.

The incorporation of chemical kinetic phenomena into the classification scheme may provide the key to higher fidelity discrimination of spectral features. The data used in the present research are the most temporally rich infrared spectral signatures available to date on the field detonation of conventional munitions. As such, these signatures offer the possibility of exploring the kinetics between spectral features and event classification. A phenomenological model has recently been developed by Gross [3] to describe the observed spectra of the detonation fireball event. The spectral model's ability to identify and extract spectral features is fairly robust. It provides fireball emissive area, temperature, particulate absorption coefficient, as well as H_2O and CO_2 concentrations. The present work is part of a research effort to gain a greater understanding of the chemical kinetic picture of a detonation event by bringing several physics-based models to bear on the problem. The 12 ms temporal resolution Fourier transform infrared spectrometer (FTS) spectra are the data sets upon which the fireball temperature are studied in the present research.

This research develops a low-dimensionality physics-based empirical model to characterize the temporal temperature evolution of combustion fireballs for improved event classification. While identification and extraction of spectral features has been studied previously, the time dependence of the fireball temperature and its relation to chemical kinetic reaction rates has not been incorporated into current classification schemes. The present research is an important step towards the leveraging of chemical kinetic phenomenology to help address the problems of event classification.

---

*joe.gordon@dtra.mil; 1-505-853-6061
†kevin.gross@afit.edu; 1-937-255-3636 x4558
‡glen.perram@afit.edu; 1-937-255-3636 x4504

Chemical, Biological, Radiological, Nuclear, and Explosives (CBRNE) Sensing XII,
Edited by Augustus W. Fountain III, Patrick J. Gardner, Proc. of SPIE Vol. 8018, 80181M

2. EXPERIMENTAL

A set of 22 novel aluminized munitions was detonated at a Department of Defense test site in Florida. Details of the test site have been reported previously. [4] The test items are 16" in. (0.41 m) tall mild steel tubes with 1/2" in. (0.013 m) thick walls and a 7" in. (0.18 m) inner diameter. The steel tubes are lined with an aluminized polyethylene (PE) annulus in the inner diameter and filled with melt-cast RDX-based high explosives (HE) with varying amounts of aluminum and paraffin wax binder. The test items are detonated 1.25 m above ground level atop a sacrificial wooden test stand. Table 1 specifies the amount of material present in the test items. The events in Table 1 and subsequent tables in this chapter are listed from least to most total number of moles in the test articles. The event nomenclature, E#, denotes chronological order in the test sequence. Paraffin wax in the HE and PE in the liner are used as reasonable surrogates for the binders.

Table 1: Composition of test articles

	Moles of Material							
Event Description	RDX	Al HE	Wax	HE Total	PE	Al Liner	Liner Total	Total
E8 - SN19	59.19	0.00	7.64	66.83	0.00	0.00	0.00	66.83
E13 - SN21	48.77	33.19	7.69	89.65	0.00	0.00	0.00	89.65
E5 - SN20	49.02	29.54	8.09	86.65	0.00	0.00	0.00	86.65
E16 - SN03	47.38	0.00	6.12	53.50	31.75	26.25	58.00	111.50
E7 - SN07	47.30	0.00	6.11	53.41	44.71	15.04	59.75	113.16
E9 - SN11	39.17	23.62	6.46	69.25	31.75	26.25	58.00	127.25
E4 - SN15	39.29	23.71	6.48	69.48	44.71	15.04	59.75	129.23
E17 - SN14	39.15	23.62	6.46	69.23	44.71	15.04	59.75	128.97
E11 - SN01	32.49	8.59	4.72	45.79	77.92	39.73	117.65	163.44
E1 - SN04	23.80	0.00	3.08	26.88	95.09	78.34	173.43	200.32
E6 - SN13	19.76	11.92	3.26	34.94	95.09	78.34	173.43	208.37
E3 - SN08	23.60	0.00	3.05	26.65	133.81	44.93	178.74	205.39

The heat capacity, heat of detonation, and heat of combustion for each event are computed using reaction stoichiometry and NIST-JANNAF Thermochemical Table heats of formation and are summarized in Table 2.

Table 2: Thermodynamic properties of test articles

	Heat Capacity		Heat of Combustion, ΔH_c				Detonation, ΔH_d		Theoretical T_o
Event Description	$C_{p,c}$ (J/K)	$C_{p,d}$ (J/K)	RDX (kJ)	HE (kJ)	Liner (kJ)	Total (kJ)	RDX (kJ)	HE (kJ)	$\Delta H_{d,RDX} / C_{p,d}$ (K)
E8 - SN19	21.06	31.66	49.97	103.72	0.00	103.72	74.03	138.14	2338
E13 - SN21	21.50	29.55	41.17	120.29	0.00	120.29	60.99	126.60	2064
E5 - SN20	21.88	30.21	41.38	120.56	0.00	120.56	61.30	130.54	2029
E16 - SN03	25.05	29.51	40.00	83.06	64.27	147.33	59.26	110.62	2008
E7 - SN07	26.94	30.46	39.93	82.90	71.98	154.87	59.19	110.40	1943
E9 - SN11	25.65	28.28	33.06	96.28	64.27	160.55	48.98	104.21	1732
E4 - SN15	27.64	29.37	33.17	96.63	71.98	168.60	49.14	104.59	1673
E17 - SN14	27.57	29.28	33.05	96.26	71.98	168.24	48.96	104.19	1672
E11 - SN01	31.35	27.98	27.42	67.07	136.86	203.93	40.63	80.60	1452
E1 - SN04	32.98	25.19	20.09	41.76	192.26	234.02	29.77	55.61	1182
E6 - SN13	33.31	24.62	16.68	48.59	192.26	240.85	24.71	52.60	1004
E3 - SN08	38.64	28.08	19.92	41.41	215.35	256.75	29.51	55.14	1051

In order to reasonably estimate stoichiometric quantities of the detonation products for the secondary combustion phase, it was hypothesized that due to the geometry of the liner, only the HE completely participates in the detonation and explosion reaction and that the liner is fragmented but only partially participates in the explosion phase. The liner does, however, fully participate in the combustion phase of the explosion. This is not an unreasonable hypothesis as analysis of high speed visible imagery suggests that the energy transferred to the shock wave of the explosion constitutes only about 2 - 15% of the expected RDX heat of detonation, assuming a constant

release of energy.[5] We can treat the combustion of the HE detonation products and combustion of the liner as two distinct processes, calculate their respective heats of combustion, and sum the two quantities to arrive at an overall heat of combustion for the event. Heat capacities are determined from reaction product species.

An instrumentation suite consisting of an 82 Hz Fourier-transform spectrometer (FTS), 100 kHz four-band radiometer, high speed digital camera operating at 3000-4200 fps, and a standard witness audio-visual digital camera collected signatures from an unobstructed standoff distance of 335 m. FTS signatures are the primary data set used for the analysis in this paper. The FTS was fitted with a 75 mrad telescope giving a 25 m diameter field-of-view (FOV) at the target. Bore-sighted video indicated that fireballs at peak area occupied only about 15 percent of the FOV and had a dwell time of about 1 s before ascending or migrating out of the FOV due to wind gusts. Of the 22 scheduled detonations, only 13 high speed digital camera signatures were successfully collected and only 12 of those 13 detonation events netted useable FTS spectra.

The ABB-Bomem MR-254 FTS operated at 82 Hz with a spectral resolution of 16 cm^{-1} = 7.71 cm^{-1}) using InSb (1800–10,000 cm^{-1}) and InGaAs (5600–10,000 cm^{-1}) detectors. Some interferograms were collected at 8 cm^{-1} resolution at a rate of 56 Hz. The interferograms were oversampled at half-HeNe wavelengths putting the Nyquist frequency at 15,802 cm^{-1}. This is well beyond the response of the InSb and InGaAs detectors and thus sufficiently avoiding aliasing of the signal reconstruction during Fourier transformation. Only the mid-infrared spectra from the InSb detector are reported in the current work.

The FTS was calibrated in the field following a method detailed by Gordon et al. [4] and Gross [3]. A low-temperature (283-353 K) wide-area blackbody (BB) source and a high-temperature (1523 K) cavity blackbody source were used to calibrate the FTS detector. The wide-area BB was positioned a few centimeters from the FTS entrance aperture and over-filled the FOV. Since instrument self-emission is important between 1750–2500 cm^{-1}, blackbody measurements enabled an accurate determination of both detector response (gain) and instrument self-emission (offset) between 1750–3000 cm^{-1}. An absolute scale for the relative gain curve between 3000–10,000 cm^{-1} was established by comparison with the gain curve previously found using the low temperature BB source where they overlap near 3000 cm^{-1}.

3. RESULTS

3.1 Spectra

In the early stages of the fireball event, the heated carbonaceous soot emits strong blackbody radiation and spectral features from selective emitters (e.g. CO, CO_2, H_2O) are masked. Figure 1 illustrates this Planckian behavior at 2 ms after detonation of an event with high aluminum content. The attenuation due to atmospheric absorption provides the primary spectral structure. Only after combustion process convert carbon to CO_2 can the selective emission be discerned.

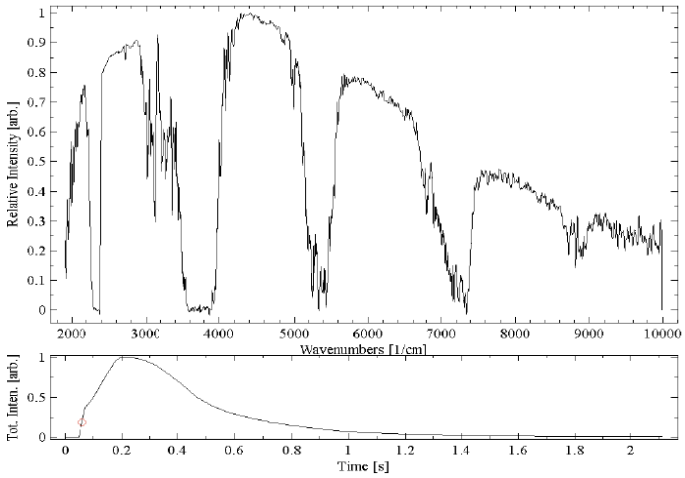

Figure 1: Early Planckian behavior of a detonation event. The spectrum corresponds to an early portion of the total mid-IR signal as shown in the bottom trace.

The emissions from Event 8 at 0.2 s and 0.8 s after detonation are provided in Figure 2, illustrating the temporal dependence of the mid-infrared spectra. The emission is relatively long lived, > 1 s. The emission from CO_2 near 2360 cm^{-1} decays more slowly than the broader continuum. The 16 cm^{-1} spectral resolution is sufficient to discern gas phase emission from CO_2 and H_2O even in the presence of significant atmospheric attenuation. There are approximately 2126 spectral samples in the spectrum.

A low-dimensionality radiative transfer model has previously been developed [3] to describe the fireball's source radiance. Assuming local thermodynamic equilibrium (LTE), negligible effects of scattering, cubic fireball geometry, fireball and atmospheric homogeneity, and large standoff distance, leads to the apparent source radiance:

$$I(\nu) = \tau_{atm}(\nu) r^2 \varepsilon(\nu) B(\nu, T) \tag{1}$$

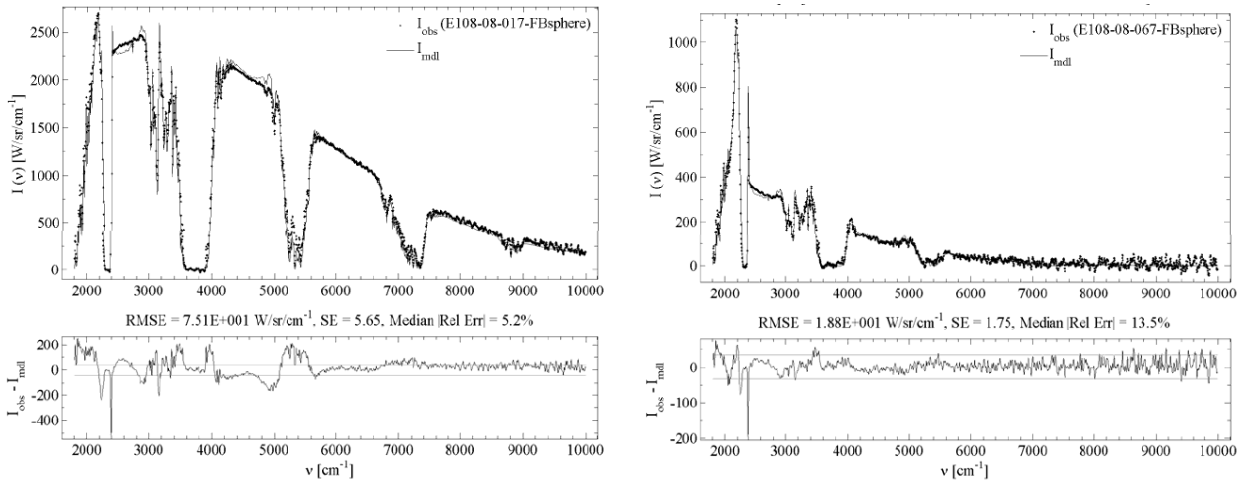

Figure 2: Mid infrared spectra for Event E8 at (a) 0.2 s and (b) 0.8 s after detonation.

where

$B(\nu;T)$ = Planckian distribution at temperature, T

$r^2 = A$ = fireball projected area

τ_{atm} = atmospheric transmission

$\varepsilon(\nu)$ = source emissivity

Absorption cross-sections, σ_i, for H_2O, CO_2 and CO at T = 275 - 3000 K are obtained from the HITRAN database [6] to express emissivity as:

$$\varepsilon(\nu) = 1 - \exp\left[-\left(\kappa_p + \sum_i \zeta_i \sigma_i(\nu, T) \right) r \right] \tag{2}$$

where

κ_p = particulate absorption coefficient

ζ_i = molecular concentration of specie i

The Boltzmann factor is included in the definition of the absorption cross-section since, under LTE, the line-strength defining the absorption cross-section varies with temperature according to the Boltzmann distribution. [3] Multiplying the source spectrum by the atmospheric transmittance and convolving it with the FTS instrument line shape realizes the

simplified radiative transfer spectral model. The state of the atmosphere and weather conditions has been previously reported. [5]

A fit of Eq. (1) to the spectrum is provided in Figure 2b, establishing a best estimate for the model parameters of T = 1030 K, r = 7.8 m, ζ_{CO2} = 6.98 x 10^{17} cm^{-3}, ζ_{H20}= 7.24 x 10^{17} cm^{-3}, and κ_p = 3.38 x 10^{-4} cm^{-1}. The median relative error in the fit is 13.5%. The full temporal dependence of the fireball temperatures determined from these spectral simulations for several events are provided in Figure 3.

For the present work, the spectral simulations are not necessary for an accurate determination of the temperatures. Two bands in the continuum region (2500-2700 cm^{-1} and 4500-4700 cm^{-1}) of the measured spectrum are compared to a theoretical Planckian distribution to determine the two-color temperature. The chosen intensity ratio exhibits a nearly linear dependence of temperature in the range T = 800 -1900 K. These two continuum region bands are chosen because they are both outside the atmospheric absorption bands as well as the emission bands from fireball plume and atmospheric constituents. A comparison of the FTS and two-color derived temperatures is provided in Figure 3.

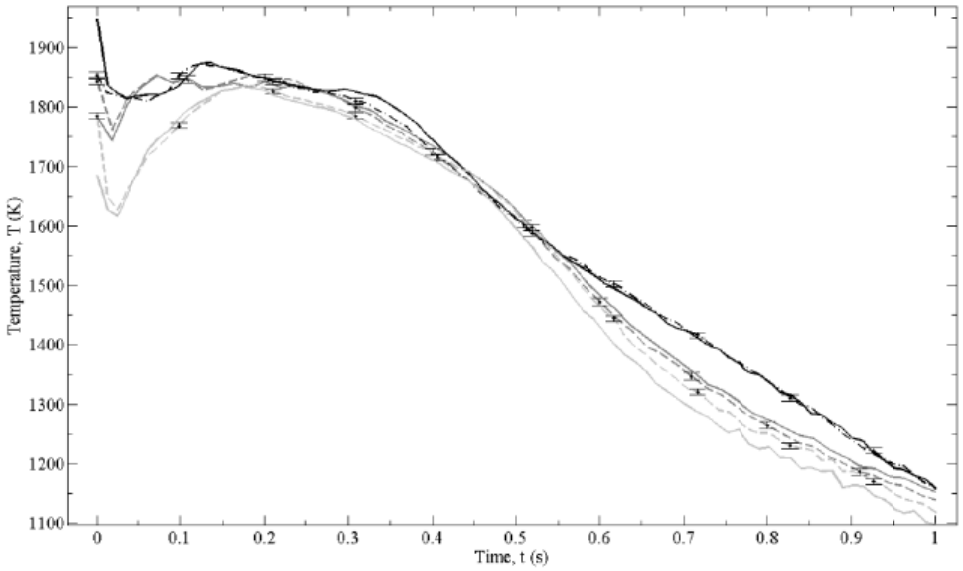

Figure 3: Comparison of temperature profiles from: (---) the spectral model of equation (1) and (—) the two-color Planckian method for events: (—) E9, (—) E4, and (—) E17.

3.2 Temperature Dynamics

The dynamics of the fireball temperature are dictated by: (1) a sudden initial temperature rise given by the energy released from the detonation into heating, (2) rapid (t < 5ms) expansion of the fireball, (3) radiative cooling, (4) turbulent mixing of the atmosphere with the detonation by products, (5) secondary combustion of detonation byproducts with atmospheric oxygen. A thorough analysis of the fluid dynamics, chemical kinetics and radiative process does not lead to the extraction of key features for classification. Instead, we chose a global, empirical model for the fireball temperature:

$$\frac{dT}{dt} = -a(T^4 - T_{atm}^4) + b(e^{-ct} - e^{-dt}) \tag{3}$$

The initial temperature, To, should be proportional to the heat of detonation, ΔH_d, relative to the total heat capacity for the detonation products, $C_{p,d}$:

$$T(t=0) = T_o \propto \frac{\Delta H_d}{C_{p,d}} \tag{4}$$

The radiative cooling is described by the Stefan-Boltzmann law:

$$a = \frac{(\varepsilon A)\sigma_{SB}}{C_{p,c}} \tag{5}$$

and σ_{SB}=5.67 x 10^{-8} W/m^2 K^4. The ambient temperature is low and may be neglected in the first term on the right hand side of Eq. (3). The high explosive is under-oxidized and the second term in Eq. (3) represents the combustion of detonation products upon mixing with atmospheric oxygen. We employ the heat capacity of the combustion products, $C_{p,c}$ to describe the temperature evolution.

The release of the heat of combustion, ΔHc, is not rapid and the first exponential term in Eq. (3) accounts for the rate of turbulent mixing. As the detonation products are fully consumed no additional heat is released and the second exponential represents this decay of combustion reagent concentration. The total heat released during secondary combustion is obtained from the time integral of the second term in Eq. (3) and is proportional to the heat of combustion:

$$\Delta H_c \propto C_{p,c}\int_0^\infty b(e^{-ct} - e^{-dt})dt = bC_{p,c}(1/c - 1/d) \tag{6}$$

Further justification for the use of the empirical equation (3) is provided in the following discussion.

Example fits of Eq. (3) for events E4 and E17 are illustrated in Figure 4. The resulting fit parameters, T_o, a, b, c, d and their associated uncertainties for each event are reported in Table 3.

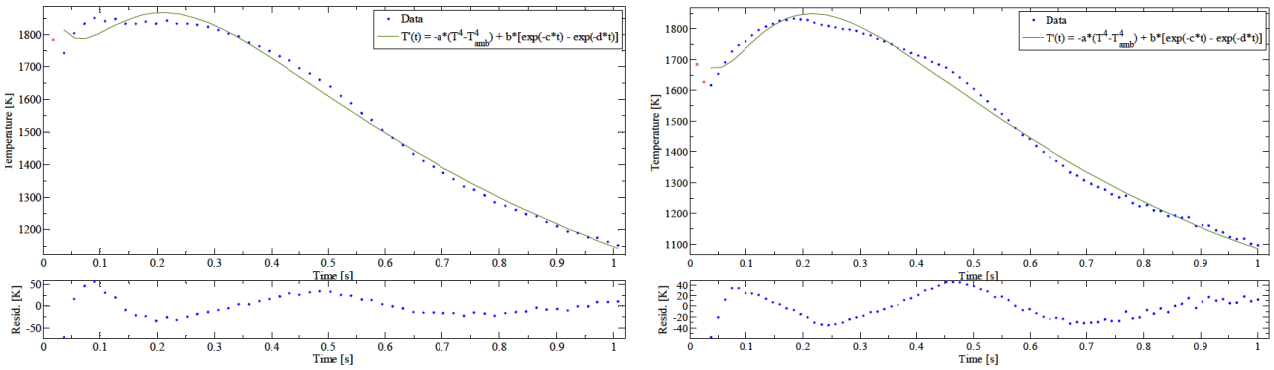

Figure 4: Evolution of two-color temperatures for events (a) E4 and (b) E17 with fit to equation (3).

Table 3: Fit parameters for temperature model

	ODE Empirical Model				
Event Description	T_o (K)	a (x10^{-10} (s^{-1} K^{-3}))	b (x10^4 (K s^{-1}))	c (s^{-1})	d (s^{-1})
E8 - SN19	1290.4 ± 34.5	8.01 ± 0.9	2.40 ± 0.7	6.25 ± 0.0003	13.85 ± 3.0
E13 - SN21	1758.1 ± 13.8	5.65 ± 0.6	3.93 ± 0.9	4.74 ± 0.0001	7.55 ± 0.6
E5 - SN20	1723.6 ± 53.2	5.66 ± 0.8	1.52 ± 0.4	5.26 ± 0.0003	18.33 ± 6.1
E16 - SN03	1631.4 ± 22.5	8.53 ± 1.1	8.40 ± 1.0	7.21 ± 0.5826	9.62 ± 0.2
E7 - SN07	1489.5 ± 32.8	7.46 ± 1.1	1.00 ± 0.2	3.24 ± 0.0001	18.64 ± 5.0
E9 - SN11	1848.3 ± 18.3	5.08 ± 0.3	2.04 ± 0.4	4.21 ± 0.4088	10.32 ± 1.6
E4 - SN15	1813.4 ± 36.7	5.08 ± 1.0	2.91 ± 1.3	4.86 ± 0.0002	9.09 ± 1.8
E17 - SN14	1673.7 ± 29.4	5.80 ± 1.2	8.11 ± 6.9	6.08 ± 0.0002	7.80 ± 1.4
E11 - SN01	1685.1 ± 62.4	5.90 ± 1.7	1.28 ± 0.6	3.65 ± 0.0002	13.56 ± 5.5
E1 - SN04	1603.7 ± 40.9	7.47 ± 1.5	2.63 + 1.2	5.29 ± 0.0013	14.70 ± 11.7
E6 - SN13	1805.1 ± 27.3	4.62 ± 0.8	3.97 ±1.5	5.05 ± 0.0001	9.03 ± 1.4
E3 - SN08	1648.4 ± 35.6	7.07 ± 1.7	2.75 ± 1.2	4.51 ± 0.0002	9.96 ± 2.1

The observed initial temperatures, T_o = 1290 – 1848 K, do not appear to correlate well with the composite HE heat of detonation. This important finding suggests that the empirical model-derived T_o is not a good parameter for event classification. For the present work, we have observed that the efficiency of converting the heat of detonation into the shock front to decrease with increased aluminum and liner content. It is not surprising that the observed initial temperatures are about 30-85% of the HE detonation energy predictions.

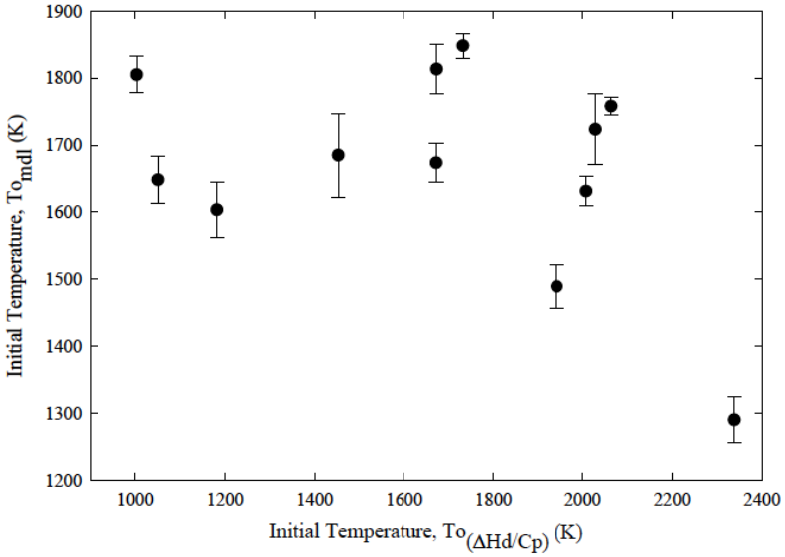

Figure 5: Scatter plot for temperatures derived from equation (3) and predicted from equation (4).

The magnitude of the radiative cooling parameter, a = 4.6 – 8.5 x 10^{-10} s^{-1} K^{-3}, is consistent with the fireball size and heat capacity. For a blackbody (ε = 1) and a typical fireball area of $A \approx 333$ m^2, and the combustion product heat capacities of Table2, equation (5) predicts the radiative cooling is described by a = 4.9 –9.0 x 10^{-10} s^{-1} K^{-3}, depending on the event heat capacity. Thus, it is estimated that time scale for the initial temperature decay is a T_o^3 = 1.93 – 4.77 s^{-1}. There is no clear correlation between the model fit parameter-derived a and calculated a values.

A strong correlation, r = 0.96, is observed between the secondary combustion fit parameters, b, c, and d and the thermodynamic properties, ΔH_c and $C_{p,c}$, as shown in Figure 6. The relationship of Eq. (6) is well supported by the experimental results and offers a potential event classification discriminator. By observing the effect for secondary combustion on the temperature decay profile, information related to the combustion heat release may be discerned. A linear fit to the data of Figure 6 provides a slope of 0.49 ± 0.1, suggesting only half of the available energy is released in the fireball.

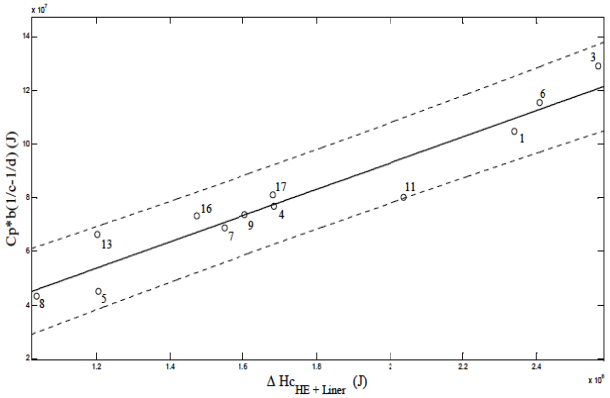

Figure 6: Correlation between predicted and observed heats of combustion from equation (6) with slope of 0.49 ± 0.1 and correlation of r = 0.96.

4. CONCLUSIONS

Mid-infrared spectra of the fireball resulting from the detonation of aluminized RDX explosives exhibit spectral features associated with CO_2, CO, H_2O and soot emission. Two spectral bands, 2500 - 2700 cm^{-1} and 4500 - 4700 cm^{-1}, have been identified with near unit emissivity to extract the evolving fireball temperature. The temperatures agree well with a simple radiative transfer model and decay from initial values of ~ 1300 – 1850 K to about 1000 K over a one second interval. The temperature profiles are adequately described by: (1) radiative cooling and (2) secondary heat release due to combustion of the under-oxidized fuel during turbulent mixing with the atmosphere. Secondary maxima are observed in the evolution of the fireball temperatures and the temperatures in excess of the radiative cooling predictions are related to the available heat of combustion. Indeed a strong correlation exists between the empirical model's estimate of the heat of combustion and the thermodynamic properties of the high explosive (RDX and aluminum) and liner. Approximately 50% of the available energy is observed in fireball temperature. The increased understanding of remote optical signatures from detonation fireballs suggests possible information for classification of event type. The initial fireball temperature exhibits no significant correlation with the heat of detonation, confirming prior suspicions that the efficiency of high explosive detonation is highly variable. However, the relative temporal dynamics of the temperature profiles do appear useful for classification. If an estimate for the heat of detonation could be determined, possibly from the shock dynamics, then the empirical value for the heat of combustion might specify the relative partitioning between high explosive content and aluminum or liner fraction. The present data samples a small selection of high explosive compositions with minimal repeatability in event type. Considerable further investigation is required to develop a complete set of key features for classification and to evaluate the probability distribution functions for various event classes.

REFERENCES

[1] Taylor, G. I., "The formation of a blast wave by a very intense explosion," *Proc. Royal Soc. A*, 201, 159 (1950).

[2] Dills, A. N., K. C. Gross, and G. P. Perram, "Detonation discrimination techniques using a Fourier Transform Infrared Spectrometer system and a Near-Infrared Focal Plane Array," *Proc. of SPIE*, 5075, 208 (2003).

[3] Gross, K. C. *Phenomenological model for infrared emissions from high-explosive detonation fireballs.* Ph.D. Dissertation, AFIT/DS/ENP/07-03, Department of Engineering Physics, Air Force Institute of Technology (2007).

[4] Gordon, J. Motos, K. C. Gross, and G. P. Perram, "Temporally-resolved, infrared spectra from the detonation of advanced munitions," in *Proc. of SPIE*, 7330, 733006 (2009).

[5] Gordon, J. Motos, *Shock wave dynamics of novel aluminized detonations and empirical model for temperature evolution from post-detonation combustion fireballs*. Ph.D. Dissertation, AFIT/DS/ENP/10-S03, Department of Engineering Physics, Air Force Institute of Technology (2011).

[6] Rothman, L. S., C. P. Rinsland, A. Goldman, S. T. Massie, D. P. Edwards, J.-M. Flaud, A. Perrin, C. Camy-Peyret, V. Dana, J.-Y. Mandin, J. Schroeder, A. Mccann, R. R. Gamache, R. B. Wattson, K. Yoshino, K. V. Chance, K. W. Jucks, L. R. Brown, V. Nemtchinov, and P. Varanasi. "The HITRAN Molecular Spectroscopic Database And HAWKS (HITRAN Atmospheric Workstation): 1996 Edition," *Journal of Quantitative Spectroscopy & Radiative Transfer*, 60, 665 (1998).